

Biocomposites based on ramie fibers and poly(L-lactic acid) (PLLA): morphology and properties

Dakai Chen^a, Jing Li^a and Jie Ren^{a,b*}

We herein report effects of morphology of PLLA and natural fiber on combination properties of biocomposites based on PLLA and ramie fibers. For this purpose, short ramie fiber (FIB), ramie fabric (FAB), PLLA film (FPLLA), and PLLA powder (PPLLA) were used to investigate the structure–property relationship of PLLA biocomposites with 30 wt% ramie fiber prepared by hot compression molding. It is revealed that mechanical properties of biocomposites are strongly dependent on the morphology of PLLA and FAB. DMA test shows that the improved storage modulus was due to the better dispersion of FIB. DSC and POM tests show that PLLA/FIB biocomposites have the highest spherulite growth rate. TGA test shows that char residue at high temperature is affected by the dispersion of PLLA and ramie fiber. SEM images exhibit the different interfacial adhesion character of FIB and FAB in the PLLA matrix after the ramie fiber treated with alkali and silane. PLLA/FAB biocomposites have not only better anti-dripping properties when burning but also better aging resistance in UV-irradiation hydrothermal aging, and which can be attributed to fiber bundle and laminated PLLA biocomposites structure. Copyright © 2010 John Wiley & Sons, Ltd.

Keywords: ramie fibers; poly(L-lactic acid); laminated PLLA biocomposites; structure–property relationship

INTRODUCTION

Considering the relative cheapness, ability to recycle, high electrical resistance, good acoustic insulating properties, strength per weight of material, and the worldwide availability, natural lignocellulosic fiber have been used as reinforcement in many thermosetting and thermoplastic resins.^[1,2] Since last year vegetal fiber reinforced biocomposites have been used as automotive parts, such as interior decorative materials and noise absorption plates, etc., for their outstanding mechanical property, lightweight and biodegradability and renewable capability.^[3] Poly(lactic acid) (PLA), a biodegradable thermoplastic polymer with high strength and modulus, has been is a perfect eco-material for many studies during the past decade for its potential in renewable engineering materials. PLA provides good aesthetics and easy processability in most equipment.^[4] In processing and manufacturing, the price and inherent brittleness are the most limitation for its wide practical applications. By addition of fiber including sisal fiber,^[5] wood fiber,^[6] bamboo fiber,^[7] nelumbo nucifera fiber,^[8] Alfa fiber,^[9] recycled newspaper,^[10] and microfibrillated cellulose,^[11] etc. or other filler material including nano-calcium carbonate,^[12] nano-titanium dioxide,^[13] and multi-walled carbon nanotube,^[14,15] etc., the mechanical properties, biodegradability, and thermal stability of the PLA based composites can be improved significantly and the price of PLA products can be reduced to some extent.

To broaden the utilization of natural fiber in PLA products, lots of properties of natural fiber reinforced PLA biocomposites have been studied. Among them most of the literature are about the

strength and modulus enhancement caused by the intrinsic property of different kinds of natural fibers and the strong interfacial adhesion between the fiber and the polymer matrix.^[16–18] The other part of works is about the exceptionally unique heterogeneous nucleation effect of natural fiber that can increase nucleation density and enhance crystallization rate.^[19,20] In our previous work, surface treatment of natural fiber can improve the thermal stability of PLA biocomposites significantly for the good adhesion of the fiber to the PLA matrix.^[21] From these results, the positive effects of natural fiber on the PLA matrix are markedly affected by the morphology of fiber and PLA matrix.

In this study, FIB, FAB, FPLLA, and PPLLA were used to investigate the structure–property relationship of biocomposites composed of PLLA and ramie fiber. The effect of morphology of ramie fiber and PLLA on mechanical properties, dynamic mechanical properties, non-isothermal and isothermal crystal-

* Correspondence to: J. Ren, Institute of Nano- and Bio-polymeric Materials, School of Material Science and Engineering, Tongji University, Shanghai 200092, P. R. China.

a D. Chen, J. Li, J. Ren

Institute of Nano- and Bio-polymeric Materials, School of Material Science and Engineering, Tongji University, Shanghai 200092, P. R. China

b J. Ren

Key Laboratory of Advanced Civil Engineering Materials, Ministry of Education, Tongji University, Shanghai 200092, P. R. China

lizaiton behaviors, thermal degradation properties, heat resistance, morphology, burning degradation process, and aging degradation phenomenon was investigated by mechanical test, dynamic mechanical analysis (DMA), polarized microscopy (POM), differential scanning calorimetry (DSC), thermogravimetric analyzer (TGA), vicat softening point tester, field emission scanning elctron (FE-SEM), UL-94 burning test, and UV-irradiation hydrothermal aging test.

EXPERIMENTAL

Materials

PPLLA and PPLLA with weight-average molecular weight of 150 kDa, polydispersity of 2 (GPC analysis) was obtained from Tong-Jie-Liang Biomaterial Co., Ltd (China). Silane coupling agent KH550 that is 3-Aminopropyltriethoxysilane, (APS) $\text{NH}_2(\text{CH}_2)_3\text{Si}(\text{OC}_2\text{H}_5)_3$, was purchased from Shanghai Yaohua Chemical Plant Co., Ltd (China). Permanganate was obtained from Shanghai Mei-xin Co., Ltd (China). Ramie fiber was purchased from Feng-Ling Co., Ltd (China), FIB has the length of 20–22 mm and FAB was used in the form of plain weave fabric. Ammonium polyphosphate (APP) ($M_n > 1000$) was obtained from Shanghai Xunshen Flame Retardant Co., Ltd., China.

Fiber surface modification

The surface hydroxyl groups of per cellulose monomeric unit are detrimental to compatibility of PLLA biocomposites. Generally speaking, there are three surface treatment methods to enhance the interfacial adhesion of these composites: (i) treatment by aqueous alkaline solution, (ii) treatment by silane coupling agent, and (iii) treatment by aqueous alkaline solution and silane coupling agent.^[22] FIB and FAB were treated with KMnO_4 acetone solution (0.4% w/v) and 0.08% silane acetone solution (weight percentage with respect to the fibers) to coordinate the cellulose's strong hydrophilic character and the PLLA's hydrophobic character and to get the good compatibility, that was called ksFIB and ksFAB. The essence of this method is to have the corrosive solution to enhance the roughness of the fiber surface and to utilize the silane coupling agent that is chemisorbed onto the fiber surface to form stable covalent bonds to the cell wall of fiber. For the hydrolysis reaction of silane coupling agent, the resultant silanol groups can react with the hydroxyl groups on the glucose units of the cellulose fiber, thereby bonding itself to the cell wall of cellulose fiber. When blended with the PLLA matrix, functional groups NH_2 on the APS would react with hydroxyl groups of the PLLA resin by hydrogen bonding interaction. Thus, chemical bonding could be established between the ramie fibers and the PLLA matrix and the interfacial properties could thus be improved. The process of cross-linking in the interface region is presented in Fig. 1.^[23]

Preparation of flame retardant PLLA biocomposites

The flame retardant APP was dried under vacuum at 80°C for 10 hr to remove moisture. The flame retardant PLLA containing 10.5 wt% APP were melt-mixed with a twin-screw extruder (LEISTRITZ, Germany) at about 170°C with a rotor speed of 25 rpm for 10 min, the product obtained was called FRPLLA. The

FRPLLA was pulverized with an electric mill (Wonder Blender, Japan), the resulted product was called FRPPLLA. FIB, ksFIB, FAB, and ksFAB were immersed in APP ethanol solution for 24 hr under agitation. Then the fibers were dried at 70°C until completely dry and FRFIB, FRksFIB, FRFAB, and FRksFAB were obtained.

Biocomposites processing

To ensure that all absorbed moisture was removed and to prevent void formation, ramie fibers, and PLLA resin were dried at 80°C under vacuum for 10 hr before processing. PLLA and ksFIB were blended using a two roll mill in the following procedure. First, one half of the PLLA was placed inside the mixing chamber for about 1 min at 30 rpm; then ksFIB was added over a period of 3 min. Then, the other half of the PLLA was added in the mixing chamber and the mixing speed was increased to 60 rpm for 5 min. The total mixing time was 10 min. The preparation of PLLA/ksFIB, FRPLLA/FRFIB, and FRPLLA/FRksFIB were conducted by the procedure same as that for PLLA/FIB. The PPLLA/ksFAB composites containing 30 wt% ksFAB were produced by press molding using the powder-stacking process. Bed lay-ups were prepared in the sections where ksFAB were stacked up with PPLLA layers on either side. The weights of PPLLA sheets and ksFAB were measured before processing so as to determine the wt% of PPLLA and ksFAB in the resulted composite. All the PLLA biocomposites obtained were then molded into sheets by hot pressing at 170°C and 20 MPa for 4 min, followed by cooling to room temperature at 5 MPa. The preparation of PPLLA/ksFAB, FRPPLLA/FRFAB, and FRPPLLA/FRksFAB were conducted by the procedure same as that for PPLLA/ksFAB. The specimens for the mechanical testing were obtained from these laminates according to ASTM standards.

Testing and characterization

Tensile strength, flexural strength, and shear strength of all samples were determined by a computer-controlled instrument and according to ASTM D3039, ASTM D790, and ASTM D256, respectively. The storage modulus, loss modulus, and loss factor (Tan Delta) of the composites specimen were measured as function of temperature (25–120°C) and were determined in three-point bending mode with a DMA Q800 Dynamic Mechanical Analyzer at a frequency of 1 Hz and at constant heating rate of 5 °C/min. DSC was performed with a TA Q100 thermal analyzer under a nitrogen flow of 20 ml/min at a heating rate of 20 °C/min. A polarized optical microscope (LEICA DMLP) equipped with a Linkam THMS 600 hot stage was used to investigate the spherulitic morphology and growth of plain PLLA, PLLA/ksFIB, and PLLA/ksFAB. The samples were first heated to 200°C for PLLA biocomposites at 100 °C/min, and held at this temperature for 3 min to destroy thermal history, then cooled at 100 °C/min to an arbitrary crystallization temperature (T_c) in the range of 100–200°C, and then held at the T_c . Annealing lasts for given time periods. TGA was performed on a Q100 thermogravimetric analyzer (Tainstsh, USA) at a heating rate of 20 °C/min, and examined under flowing air (80 ml/min) over a temperature range from ambient to 700°C. The vicat softening temperature was tested according to ASTM D1525 Standard. The surface morphologies of kfAB were observed by Quanta 200 FEG (FEI Company) with field emission gun and accelerating voltage of 10 kV was used to collect SEM images of the surface of ramie

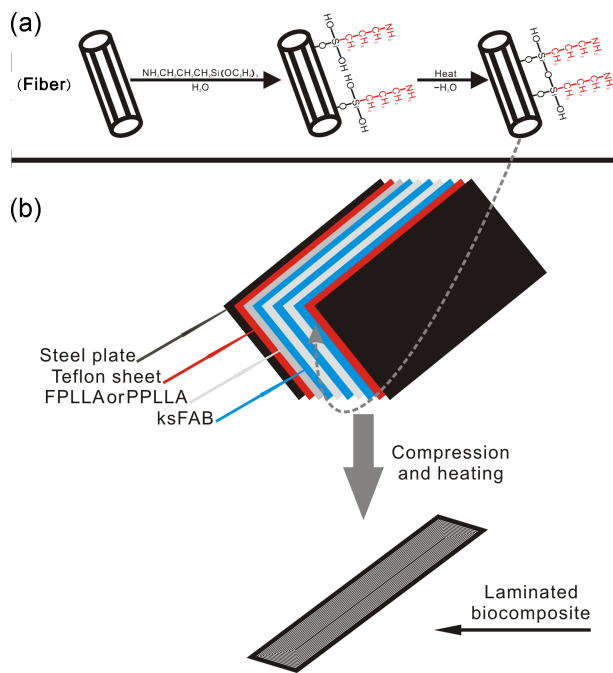


Figure 1. (a) Grafting treatment with silane coupling agent on the surface of ramie fiber and (b) fabrication procedure of the laminated PLLA biocomposites. This figure is available in color online at wileyonlinelibrary.com/journal/pat

fibers. The morphologies of the fractured surfaces of the PLLA biocomposites were observed by a scanning electron microscopy (SEM) (Hitachi S-2360N, Tokyo, Japan).

Burning degradation and aging degradation tests

UL-94 test was performed by vertical burning test instrument (CZF-2) (Jiangning, China) and the specimen size was $125 \times 13 \times 3 \text{ mm}^3$. In the measurement, samples were vertically exposed to a Bunsen burner flame for 10 sec. If the flame extinguished, another 10 sec was employed. UL-94 ratings of samples were determined by total burning time of the two ignitions according to ASTM D-3801.

Aging test was made according to GB/T 16422.3 standards. Light source for aging testing chamber is UV-B313 fluorescent ultra-violet lamp, discontinuous illumination was used as working model. The time of aging cycle was 12 hr and one cycle was divided into two phases. Phase 1 simulated the exposure of sunlight with the radiation exposure time of 8 hr at $60 \pm 1^\circ\text{C}$. The phase 2 simulated the effect of dew in nature with irradiation-free condensation exposure time of 4 hr at $50 \pm 1^\circ\text{C}$. The intensity of UV-irradiation was 0.6 W/m^2 and the samples were taken out after 7, 14, and 21 days to measure mechanical properties.

RESULTS AND DISCUSSION

Mechanical properties of PLLA biocomposites

Figure 2 shows the mechanical properties of ramie fiber reinforced PLLA biocomposites. The mechanical strength is significantly improved by adding ramie fiber compared to the

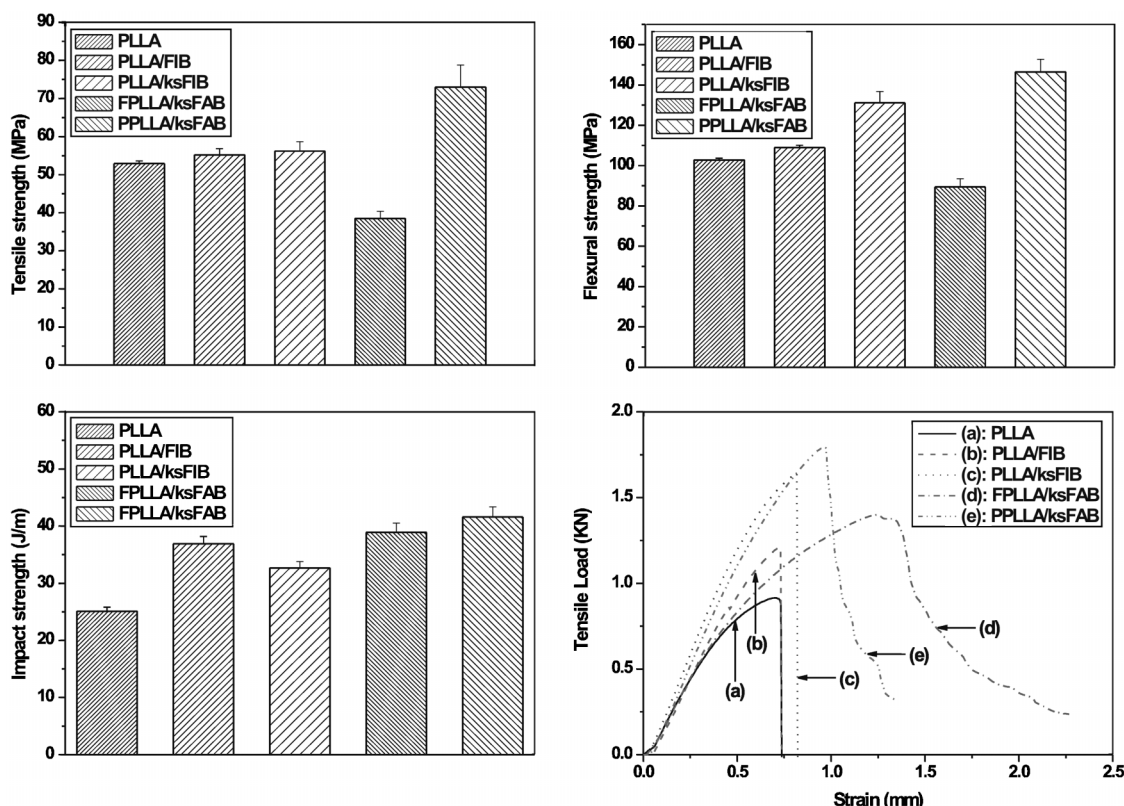


Figure 2. Mechanical properties of PLLA and PLLA biocomposites.

plain PLLA. The ksFIB and ksFAB are responsible for a well interfacial PLLA/ramie fiber adhesion, which explains an increase in tensile and flexural strength of PLLA/ksFIB, FPLLA/ksFAB, and PPLLA/ksFAB. The tensile and flexural strength of PLLA is increased by 20% because of the two-dimensional structure of ksFAB. The flexural strength of the PLLA biocomposites is also improved. The maximum tensile strength is as high as 73 MPa (PPLLA/ksFAB). As shown in Fig. 2, the PPLLA/ksFAB can have the highest notched izod impact strength of 41.6 J/m. The ksFIB and ksFAB have a lasting effect on fiber stiffness. And the fiber-fiber interaction as well as fiber-matrix interaction can play a more fundamental role in transferring the stress from the PLLA matrix to ramie fibers. For toughness is the major factor that controls the impact strength, the amount of energy required for breaking increase by adding ramie. The two-dimensional structure of ksFAB plays a more important role in the impact strength increase compare to the dispersion of ksFIB in PLLA biocomposites. The improvement of tensile and flexural strength is due to the improved fiber-matrix adhesion by the surface treatments. Natural and artificial impurities can be removed and a rough surface topography is obtained by surface treatments. The toughness of PLLA biocomposites is improved because of high toughness of ramie fibers. However, the toughness of ramie fibers may be reduced by surface treatments, which make the impact strength of PLLA/ksFIB lower than that of PLLA/FIB. For the fiber bundle structure of ramie fabric, most of ramie fibers in FAB will not be damaged by surface treatments, and PPLLA/ksFAB shows the high impact strength. The improvement of PLLA/ramie fiber interfacial adhesion does not necessarily increase the impact performance of PLLA biocomposites. The PLLA morphology plays an important role in improving the mechanical properties of the PLLA biocomposites, for PPLLA has the better resin permeability than FPLLA in PLLA biocomposites.

Dynamic mechanical properties

The temperature curves of storage modulus, loss modulus, and loss factor are shown in Fig. 3. It shows that the storage modulus of PLLA/ksFIB is higher than that of the FPLLA/ksFAB and PPLLA/ksFAB due to the reinforcement effect imparted by the well-distributed ksFIB. As seen in Fig. 3(A), the PPLLA/ksFAB has higher storage modulus than that of FPLLA/ksFAB. This suggests that the interfacial adhesion between the ramie fiber and PLLA matrix is higher than that of FPLLA/ksFAB. Therefore, the transfer property of PLLA resin is a key factor for having high modulus in PLLA biocomposites. The storage modulus increases by 80 and 52% in the cases of PLLA/ksFIB and PPLLA/ksFAB, respectively, compared to FPLLA/ksFAB composites at 25°C. This phenomenon is attributed to the improved interfacial adhesion between the PLLA matrix and the ramie fiber. As shown in Fig. 3(A), the storage modulus decreases with the increase in temperature in the cases of all samples, and there was a significant fall in the regions between 50 and 70°C. There is a longer plateau on the storage modulus of PLLA/ksFIB than that for PLLA/ksFAB where the softening temperature is increased from about 48°C for PLLA/ksFAB to 57°C with PLLA/ksFIB, which implies an increase in thermal stability of the plain PLA matrix with the addition of ksFIB and it is further increased if the composite is crystallized. These DMA results show important variations of main relaxation temperature, which can be linked both to interactions resulted in a decrease of chain mobility and to a regular reinforcing effect. These results are consistent with

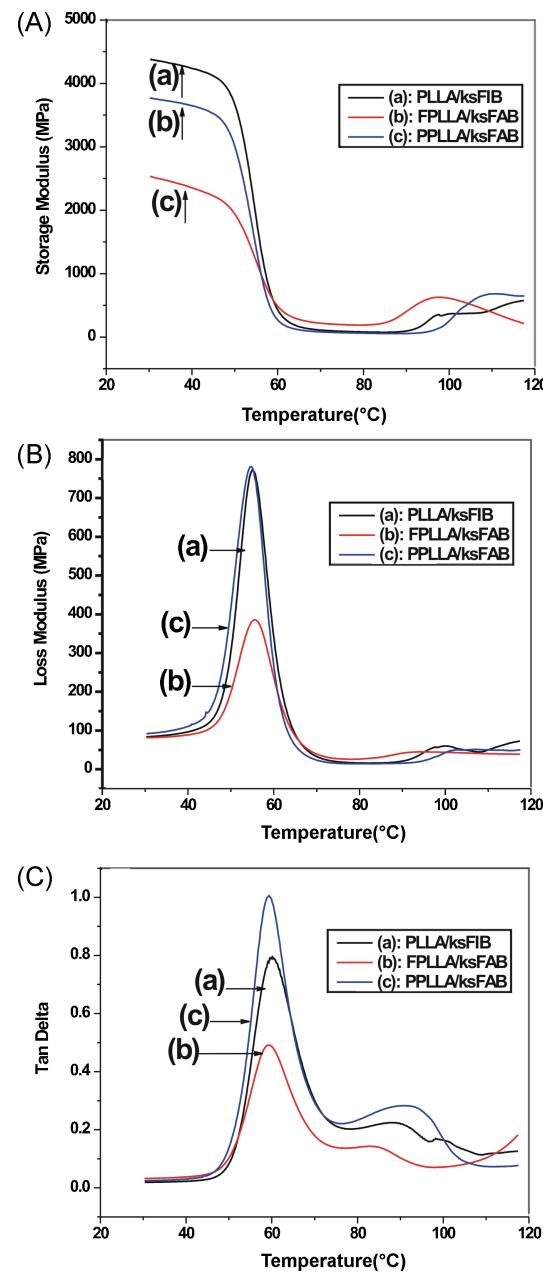


Figure 3. DMA results of the PLLA composites. This figure is available in color online at wileyonlinelibrary.com/journal/pat

the static mechanical behavior, which vary with different ramie fiber morphology. In the present investigation the relaxation of PLLA/ksFIB, FPLLA/ksFAB, and PPLLA/ksFAB have also been studied from the loss modulus curves shown in Fig. 3(B). The glass transition temperature (T_g) which is derived from loss modulus curves is interpreted as the peak of the loss modulus curves obtained during dynamic mechanical testing. The T_g of ksFIB/PLLA is shifted to higher temperature because of the nucleation effect of ksFIB in PLLA matrix. The shifting of T_g to higher temperatures can be associated with the decreased mobility of PLLA chains, which indicates that enhanced interfacial adhesion between ramie fiber and PLLA matrix is achieved by the distribution of PLLA and filler. This can be explained based on the retardation in the relaxation of amorphous regions due to the

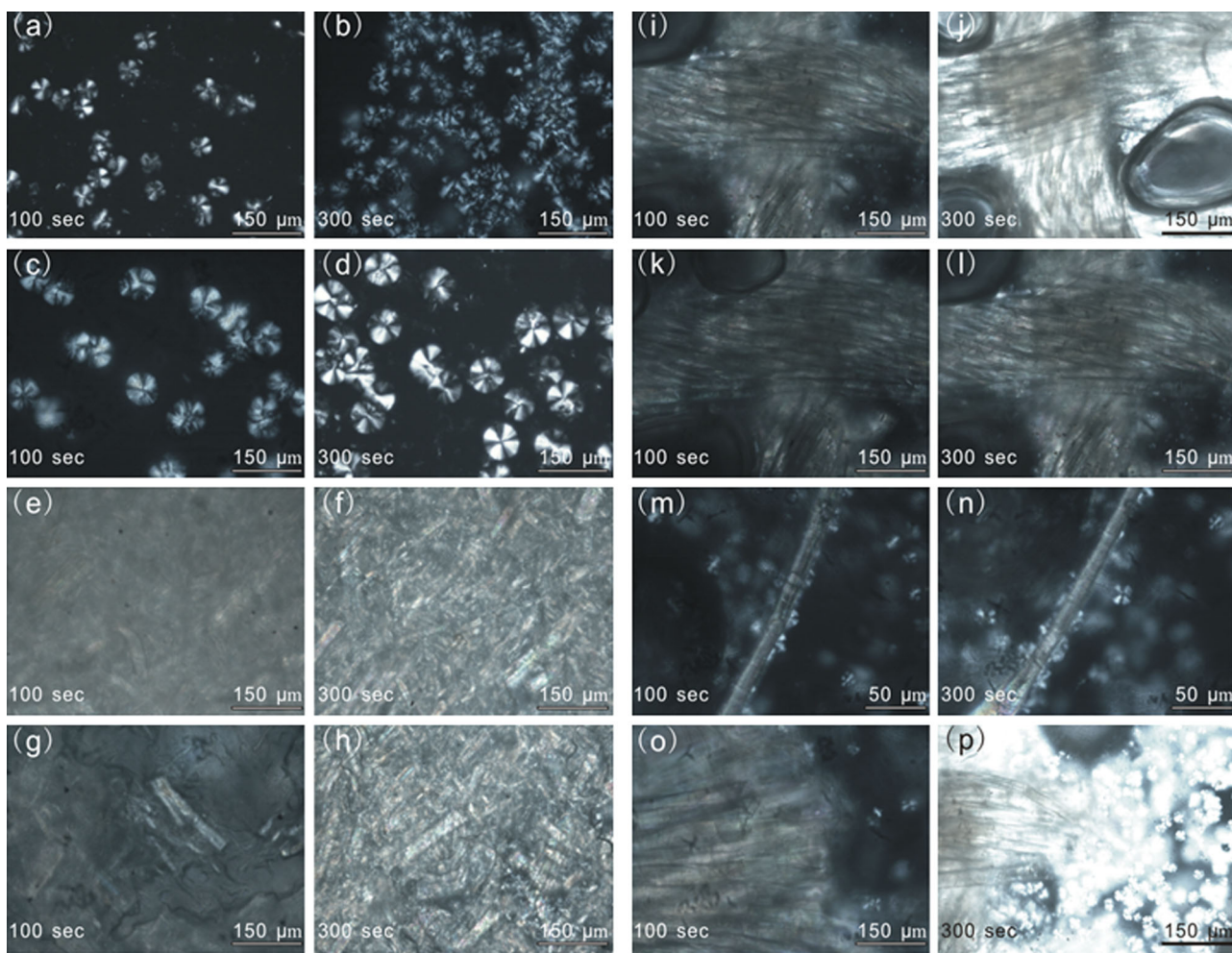


Figure 4. Optical micrographs of plain PLLA (a–d), PLLA/ksFIB (e–h), PLLA/ksFAB (i–l), single ksFIB in PLLA matrix (m, n), and marginal area of ksFAB in PLLA matrix (o, p) isothermally melt-crystallized at 120°C (a, b, e, f, i, j, m, n, o, p) and 140°C (c, d, g, h, k, l). This figure is available in color online at wileyonlinelibrary.com/journal/pat

physical interaction with the reinforcing phase and the crystalline regions of the PLA matrix. Figure 3(C) shows the loss factor ($\tan \delta$) of the ramie fiber/PLLA composites as a function of temperature. As seen in Fig. 3(C), the contribution of ramie fiber to the damping is extremely low compared to that of the PLLA matrix. This suggests that the combined attenuation of ramie fiber reinforced composites would be mainly caused by the molecular motion of PLLA and the interaction at the PLLA/ramie fiber interface.

Spherulite morphology and growth

The spherulite morphology of pure PLLA, PLLA/ksFIB, and PLLA/ksFAB isothermally melt-crystallized at 120 and 140°C were observed by polarizing optical microscopy (POM), and the results are shown in Fig. 4. Compared to the characteristic "Maltese cross" spherulite morphology of pure PLLA as shown in Fig. 4(a)–(d), it is obvious that with the addition of ksFIB the nucleation density increases greatly and the spherulite size drops drastically at both 120 and 140°C, which confirms that the ksFIB can significantly accelerate the nucleation and crystallization of PLLA. On the other hand, the nucleation density reduces and the spherulite size increases with the increase of the crystallization temperature, as shown in Fig. 4(e)–(h). Figure 4(i)–(l) show

polarized light microscopic micrographs of ksFAB embedded in molten PLLA. With the addition of ksFAB the nucleation density decreases greatly and it is shown that the morphology of ramie fiber is directly bound up with the crystalline of PLLA. As shown in Fig. 4(m) and (n), ksFIB acts as nucleating agent for PLLA as nucleation occurs preferentially along the fiber axes. The transcrystalline layer is not symmetrically developed around the ksFIB and the thickness of the transcrystalline layer increases with time. Besides, the nucleation density on ksFIB surface is higher than that on ksFAB. In the molten state of PLLA, crystalline lamellae grow radially outwards from a small stable crystal and then successive branching. When the spherulites impinge onto each other then the spherulite growth stops. As shown in Fig. 4(o) and (p), in the compact structure of ksFAB in PLLA matrix the PLLA chains are confined to a narrow area and crystalline lamellae cannot grow.

Vicat softening temperature

The vicat softening temperature reflects the point of softening to be expected when a material is used in an elevated temperature application. Vicat softening temperature of PLLA/ksFIB, FPLLA/ksFAB, and PPLLA/ksFAB are shown in Fig. 5. As seen in Fig. 5,

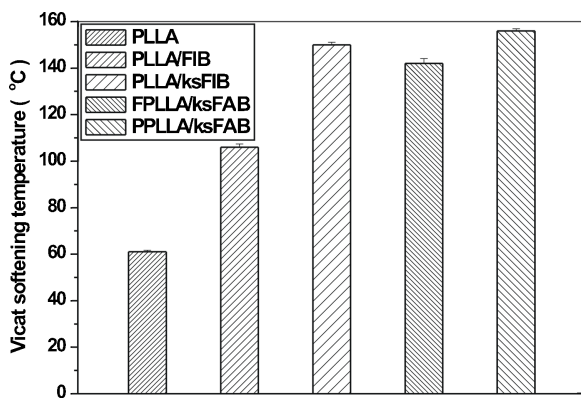


Figure 5. Vicat softening temperature of PLLA and PLLA biocomposites.

vicat-softening temperature of PLLA/ksFIB increases significantly compared with that of FPLLA/ksFAB and PPLLA/ksFAB. The crystallinity enhances the heat resistance of PLLA/ksFIB. The heat resistance improvement of FPLLA/ksFAB and PPLLA/ksFAB might be due to ksFAB reinforcement that prevents the deformation of the PLLA biocomposites. Vicat softening temperatures of PPLLA/ksFAB is higher than that of FPLLA/ksFAB. This improvement is mainly derived from the increase in the interaction between PLLA matrix and ksFAB. The results of vicat softening point are in agreement with the results of TGA.

Morphology of surface-treated fibers and PLLA biocomposites

As shown in Fig. 6(a) and (b), the FIB and ksFIB show the well dispersity in PLLA matrix. With the melt-mixed process of twin-screw extruder, PLLA and the cellulose fiber can show the well dispersion in PLLA biocomposites, the effect of the covalent bond between PLLA and the cellulose fiber will not considerably improve the dispersion of the fiber into the PLLA matrix. Figure 7 shows the surface features of the ramie fiber and the tensile fracture surface features of PLLA biocomposites. A comparison between FIB and ksFIB reveals topographical changes because of the removal of low molecular weight compounds resulted in a formation of a rougher surface. One of the consequences of the topographical change is an increase in the surface area. SEM

micrographs of the fracture surface of PLLA/FIB, PLLA/ksFIB, PPLLA/FAB, and PPLLA/ksFAB are shown in Fig. 7(f)–(k). The fiber pull out in Fig. 7(f) is an indication of low PLLA/FIB adhesion. Figure 7(g) shows the presence of aggregation at the surface and fiber breakage, and it clearly indicates that surface-treatment facilitates good adhesion between PLLA matrix and ksFIB. Figure 7(j) shows that ksFAB are well trapped by the PPLLA matrix when compared FAB in PPLLA/FAB. The ramie fiber has been covered with a thin layer of the matrix bonding the fiber surface to the matrix, and thus better stress transfer could be expected. Figure 7(k) shows the interfacial adhesion between the ramie fiber bundles as well as the individual fibers and the matrix. This improved adhesion leads to a significant increase in flexural properties. Figure 8 shows the aspect of interface minutely. As shown in Fig. 8(a) and (c), the untreated cellulose fibers show the poor adhesion strength with PLLA matrix in PLLA/FIB and PPLLA/FAB. While in PLLA/ksFIB and PPLLA/ksFAB, the treated cellulose fibers show the well adhesion strength with PLLA matrix. The adhesion strength between ramie fiber and PLLA matrix is very important to the mechanical properties of PLLA biocomposites. Figure 9(a)–(d) show affects of morphology of PLLA on the lamellar structure of PLLA biocomposites. In hot compression molding, the fiber bundle can make spacing between the layers larger, but PPLLA can avoid this process and make the fiber bundle slide to the other area. Compared to FPLLA, PPLLA has the larger specific surface area and it will improve the adhesion with ramie fiber.

Thermal degradation properties

PLLA is the material that is very sensitive to heat. There is noticeable thermal degradation when the temperature is over 200°C. From Fig. 10, it can be seen that the PLLA biocomposites with FIB show lower degradation temperature than that of PLLA/ksFIB. The chemical bond between PLLA and ksFIB could enhance the interfacial adhesion and the thermal degradation temperature increases consequently. However, the thermal degradation temperatures of FPLLA/ksFAB and PPLLA/ksFAB are lower than that of the PLLA/ksFIB. The result might be due to the dispersibility of ramie fiber in PLLA matrix causing that the content of ramie fiber in PLLA/ksFIB is lower than that in FPLLA/ksFAB and PPLLA/ksFAB. It implies that the dispersion of PPLLA in net-structure of ksFAB is better than that of FPLLA.

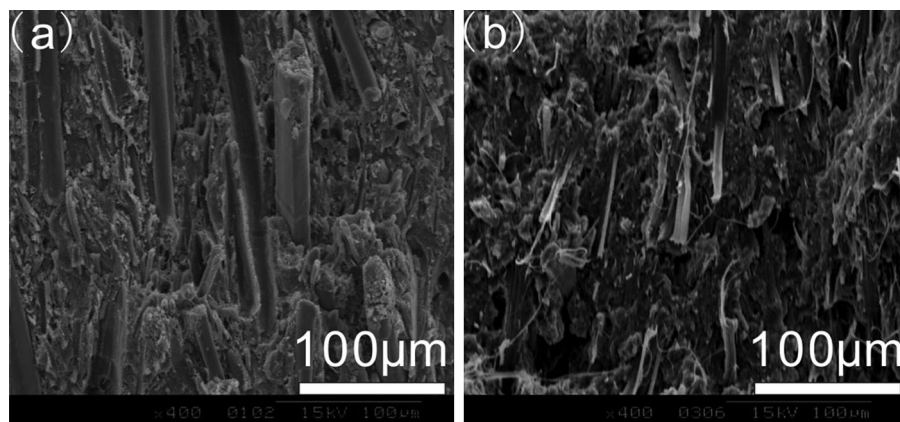


Figure 6. SEM micrographs of the dispersity of short ramie fiber in PLLA matrix: (a) PLLA/FIB and (b) PLLA/ksFIB.

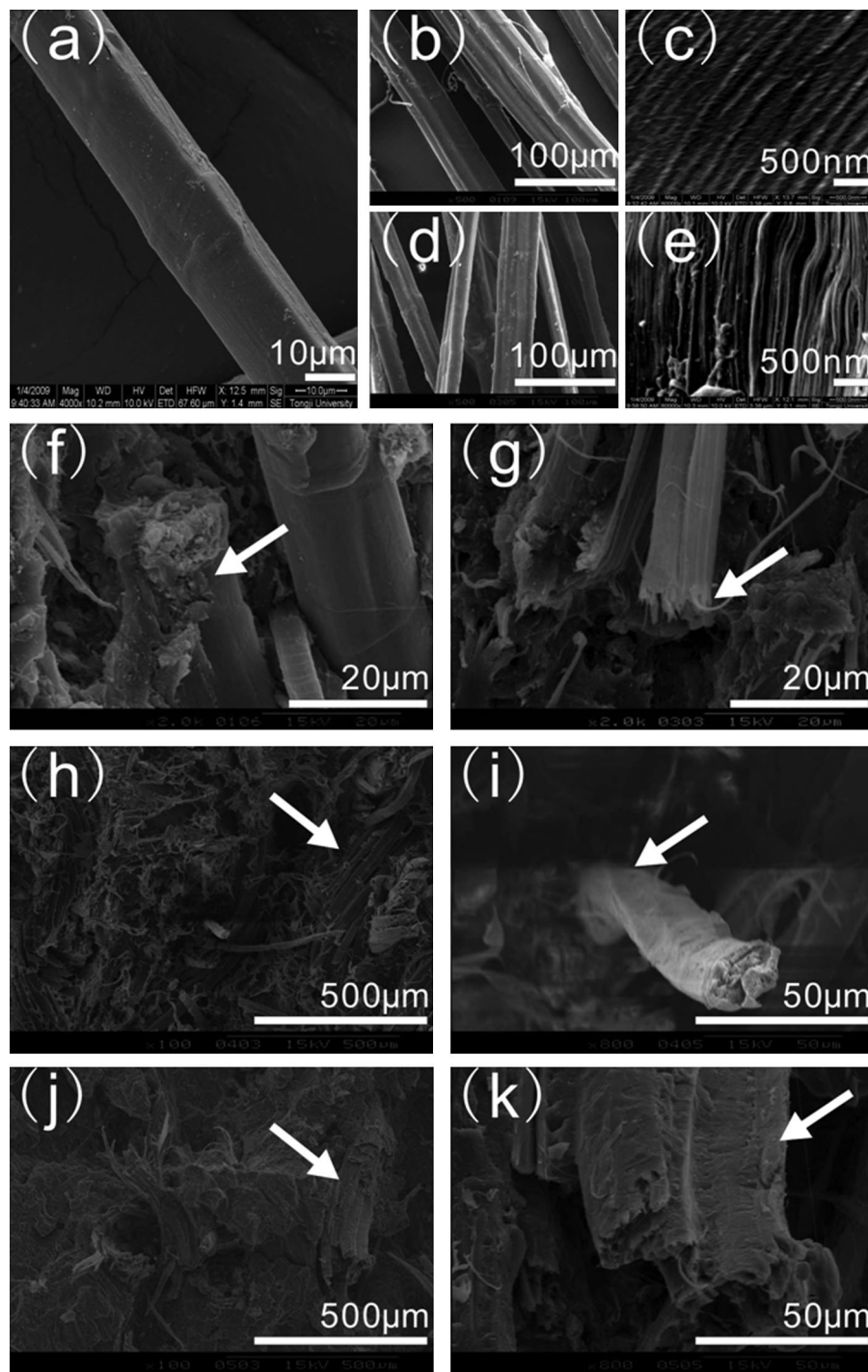


Figure 7. SEM micrographs of the surface features of ramie fiber: (a–c) FIB, (d, e) kFIB and SEM micrographs of the tensile fracture surface features of PLLA biocomposites, (f) PLLA/FIB, (g) PLLA/ksFIB, (h, i) PPLLA/FAB and (j, k) PPLLA/ksFAB.

The results of UL-94 burning tests are presented in Fig. 11(a)–(d). PLLA/ksFIB and PPLLA/ksFAB can all not be classified by UL-94 rating. The surface of combustion product of PLLA/ksFIB is smooth and most of the ramie fiber and PLLA matrix are burnt out for PLLA and ramie fiber are all flammable materials. But ramie fiber can act as charring agent, which causes a marked increase in the thickness of char layer on the surface of PLLA/ksFIB. In the UL-94 tests, the dripping phenomenon of PLLA/ksFIB

is very obvious. Figure 11(c) shows the simulation of combustion process and structure of charring layer of PLLA/ksFIB and PPLLA/ksFAB. The surface of the combustion product of PPLLA/ksFAB presents a relatively dense net-structure char layer, and this net-structure char layer provides the PPLLA/ksFAB with well anti-dripping properties in burning test. Under the synergistic effect of flame retardant, these dense char can act as a barrier against heat and mass transfer between flame zone and

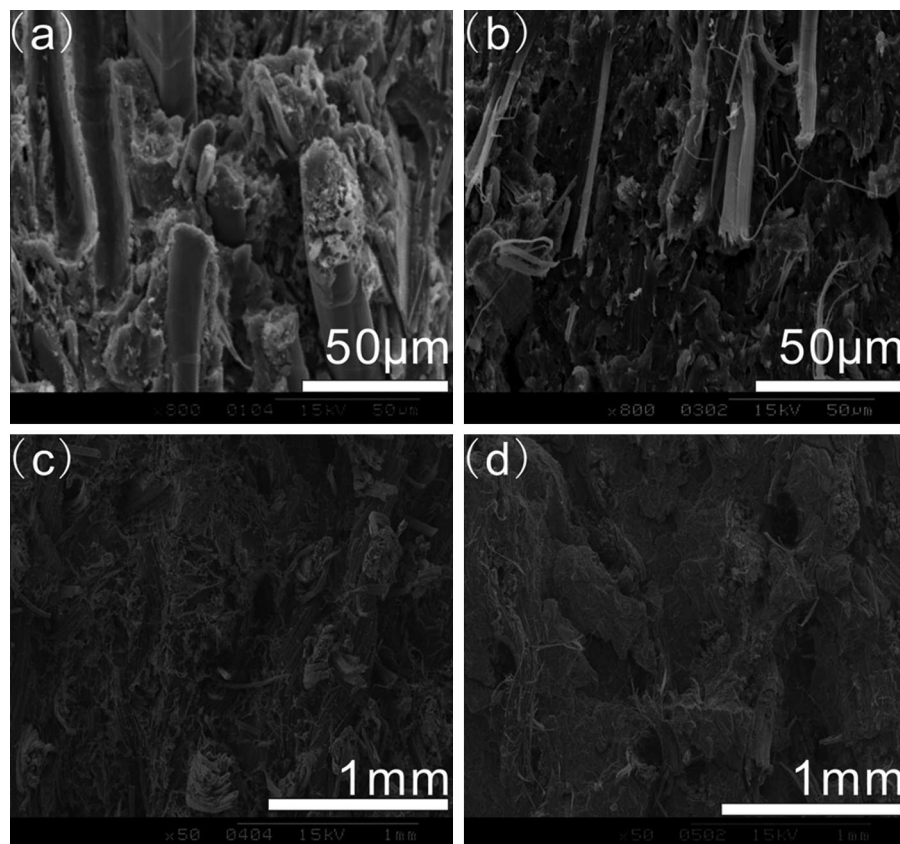


Figure 8. SEM micrographs of the adhesion between ramie fiber and PLLA matrix: (a) PLLA/FIB, (b) PLLA/ksFIB, (c) PPLLA/FAB, and (d) PPLLA/ksFAB.

underlying materials, thus hindering the continuous combustion of materials.

UV-irradiation hydrothermal aging degradation properties

The sharp decline in mechanical strength of PLLA biocomposites at the earlier stage of aging tests is caused by combined action of UV-irradiation and hydrothermal environment. As seen in Fig. 12(a), the mechanical drop rate of PPLLA/ksFAB is less than FPLLA/ksFAB and PLLA/ksFIB. In aging test, the moisture absorption of PLLA biocomposites is very important to the stabilization of mechanical properties. The diffusion of water

molecule inside the minute crevices between polymer chains, the capillary transport into the gaps and flaws at the interfaces between ramie fiber and PLLA are caused by incomplete wettability and impregnation and the transport by micro-fracture in the PLLA matrix takes place during the compounding process. In the process of two-roll mill, there are more polymer minute crevices, interface gaps and matrix micro-fracture than that in hot compression molding of FPLLA/ksFAB and PPLLA/ksFAB. Because of the better dispersibility of PPLLA in net-structure of ksFAB, there are less interface gaps than that in FPLLA/ksFAB. Because of low moisture absorption of PPLLA/ksFAB the PLLA/ramie fiber interfacial properties can be maintained, which is the main

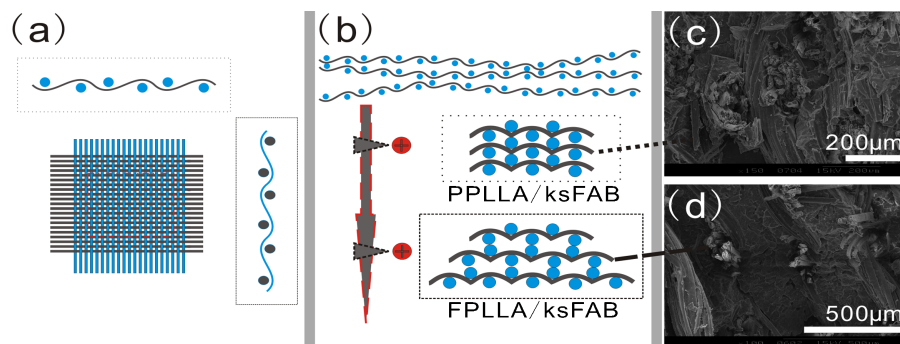


Figure 9. (a) Structural model of ramie plain weave fabric and (b-d) cross section structural model and the layer to layer spacing of PPLLA/ksFAB and FPLLA/ksFAB. This figure is available in color online at wileyonlinelibrary.com/journal/pat

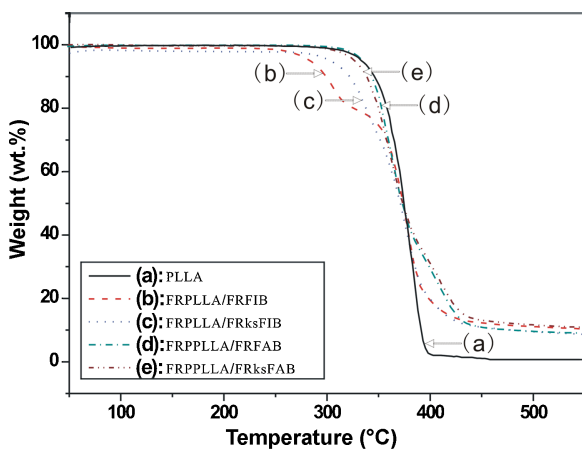


Figure 10. TGA results of the PLLA and PLLA biocomposites. This figure is available in color online at wileyonlinelibrary.com

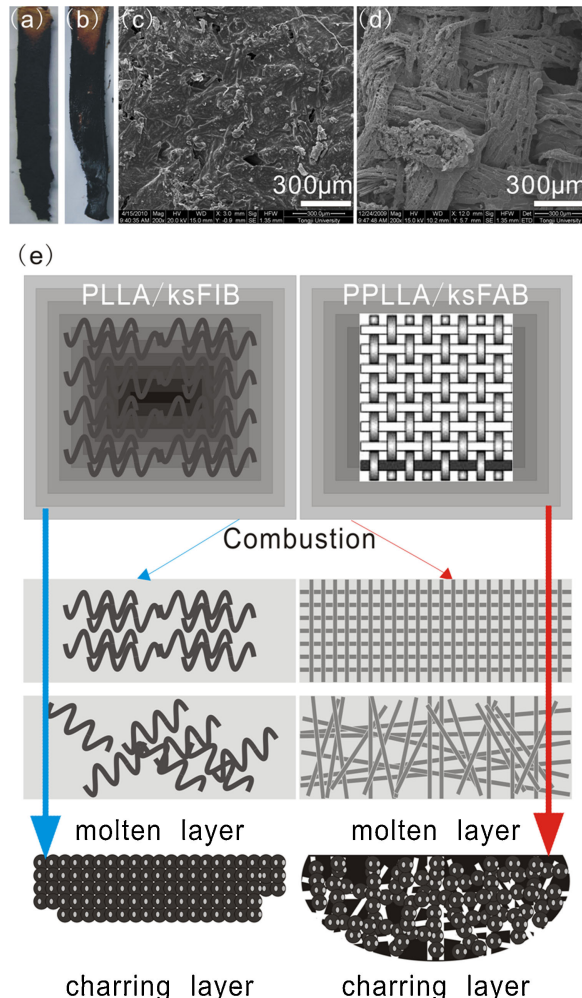


Figure 11. Samples after burning test: (a) PLLA/ksFIB and (b) PPLLA/ksFAB, SEM micrographs of outer surfaces of intumescence char obtained from biocomposites after UL-94 test; (c) PLLA/ksFIB and (d) PPLLA/ksFAB, (e) combustion process and structure of charring layer. This figure is available in color online at wileyonlinelibrary.com/journal/pat

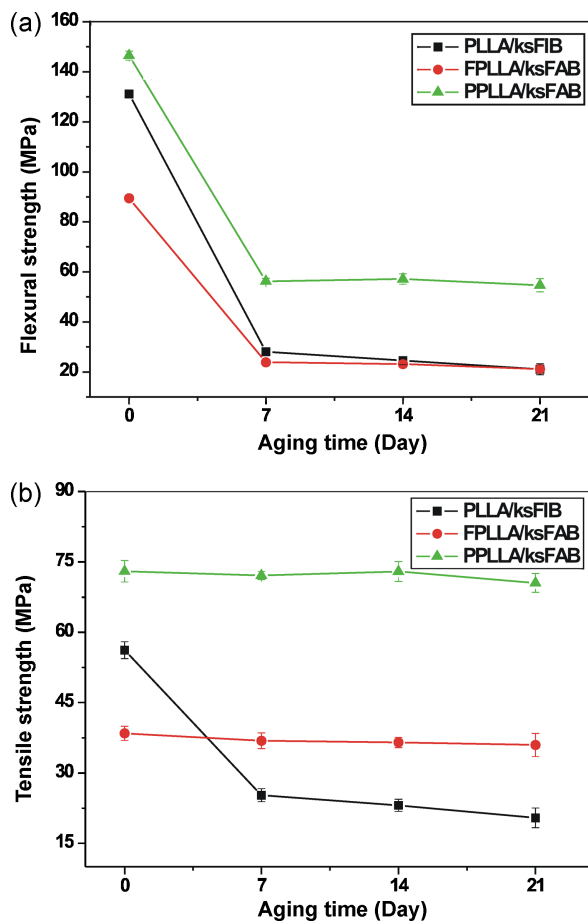


Figure 12. Change of mechanical properties of PLLA/ksFIB, FPLLA/ksFAB, and PPLLA/ksFAB after aging test: (a) flexural strength and (b) tensile strength. This figure is available in color online at wileyonlinelibrary.com/journal/pat

causing high drop rate of the flexural strength of PLLA biocomposites. As shown in Fig. 12(b), because of the high moisture absorption the tensile strength drop of PLLA/ksFIB is accelerated. Cellulose fiber's water absorption induces the swelling property of ramie fibers, which reduce the interfacial adhesive strength in critical area of cellulose fiber and PLLA matrix and present the large difference of drop curve in the mechanical properties of PLLA biocomposites. The two-dimensional structure of ksFAB is not damaged in the UV-irradiation hydrothermal aging test, which is the main reason for retention of tensile strength of FPLLA/ksFAB and PPLLA/ksFAB.

CONCLUSION

The mechanical properties, dynamic mechanical properties, crystallinity, thermal stability, heat resistance, burning anti-dripping, and aging resistance of ramie fiber/PLLA biocomposites are greatly influenced by the morphology of fiber and PLLA. The generation of PPLLA and ksFAB improves the mechanical properties of PLLA biocomposites significantly as compared to plain PLLA because the two-dimensional structure of ramie fiber and the smaller layer-to-layer spacing are caused by better dispersion of PPLLA in net-structure of ksFAB. Storage modulus of PLLA biocomposites is improved for the better dispersion of ksFIB

caused by surface treatment and ksFIB can significantly accelerate the nucleation and crystallization of PLLA. The chemical surface treatment can enhance the interfacial adhesion and the thermal degradation temperature rises consequently. The crystallinity and reinforcing of ksFIB can also enhance the heat resistance of PLLA/ksFIB. The investigation indicates that interfacial adhesion, dispersion of ramie fiber, and structure of PLLA matrix and ramie fiber are the main factors that affect the combination property of PLLA biocomposites. Among them, the two-dimensional structure of ramie fiber plays a critical role for anti-dripping properties in burning test. Besides, the interfacial adhesion and dispersion of PLLA matrix and ramie fiber play a significant role for aging resistance in UV-irradiation hydro-thermal aging test. This comprehensive study of ramie fiber reinforced PLLA biocomposites should also be referred for some other biocomposites systems.

Acknowledgements

This work is supported by the National High Technology Research and Development Program of China (No. 2006AA02Z248), the Program of Shanghai Subject Chief Scientist (No. 07XD14029) and the fund of Shanghai International co-operation of Science and Technology (No. 075207046).

REFERENCES

- [1] K. Oksman, M. Skrifvars, J. F. Selin, *Compos. Sci. Technol.* **2003**, *63*, 1317–1324.
- [2] M. J. John, S. Thomas, *Carbohyd. Polym.* **2008**, *71*, 343–364.
- [3] M. M. Farag, *Mater. Design* **2008**, *29*, 374–380.
- [4] L. T. Lim, R. Auras, M. Rubino, *Prog. Polym. Sci.* **2008**, *33*, 820–852.
- [5] P. V. Joseph, M. S. Rabello, L. H. C. Mattoso, K. Joseph, S. Thomas, *Compos. Sci. Technol.* **2002**, *62*, 1357–1372.
- [6] M. Bengtsson, P. Gatenholm, K. Oksman, *Compos. Sci. Technol.* **2005**, *65*, 1468–1479.
- [7] K. Okubo, T. Fujii, E. T. Thostenson, *Compos. A* **2009**, *40*, 469–475.
- [8] D. Liu, G. T. Han, J. C. Huang, Y. M. Zhang, *Carbohyd. Polym.* **2009**, *75*, 39–43.
- [9] R. Belhassen, S. Boufi, F. Vilaseca, J. P. Lopez, J. A. Mendez, E. Franco, M. A. Pelach, P. Mutje, *Polym. Adv. Technol.* **2009**, *20*, 1068–1075.
- [10] M. S. Huda, L. T. Drzal, A. K. Mohanty, M. Misra, *Compos. Sci. Technol.* **2006**, *66*, 1813–1824.
- [11] A. N. Nakagaito, H. Yano, *Cellulose* **2008**, *15*, 555–559.
- [12] S. Y. Gu, C. Y. Zou, K. Zhou, J. Ren, *J. Appl. Polym. Sci.* **2009**, *114*, 1648–1655.
- [13] H. T. Liao, C. S. Wu, *J. Appl. Polym. Sci.* **2008**, *108*, 2280–2289.
- [14] C. S. Wu, H. T. Liao, *Polymer* **2007**, *48*, 4449–4458.
- [15] J. T. Yoon, Y. G. Jeong, S. C. Lee, B. G. Min, *Polym. Adv. Technol.* **2009**, *20*, 631–638.
- [16] D. Ray, B. K. Sarkar, S. Das, A. K. Rana, *Compos. Sci. Technol.* **2002**, *62*, 911–917.
- [17] A. K. Mohanty, L. T. Drzal, M. Misra, *J. Adhes. Sci. Technol.* **2002**, *16*, 999–1015.
- [18] M. F. Rosa, B. S. Chiou, E. S. Medeiros, D. F. Wood, T. G. Williams, L. H. C. Mattoso, W. J. Orts, S. H. Imam, *Bioresour. Technol.* **2009**, *100*, 5196–5202.
- [19] P. J. Pan, B. Zhu, W. H. Kai, S. Serizawa, M. Iji, Y. Inoue, *J. Appl. Polym. Sci.* **2007**, *105*, 1511–1520.
- [20] L. Suryanegara, A. N. Nakagaito, H. Yano, *Compos. Sci. Technol.* **2009**, *69*, 7–8.
- [21] T. Yu, J. Ren, S. M. Li, H. Yuan, Y. Li, *Compos. A* **2010**, *41*, 499–505.
- [22] M. J. John, B. Francis, K. T. Varughese, S. Thomas, *Compos. A* **2008**, *39*, 352–363.
- [23] M. S. Huda, L. T. Drzal, A. K. Mohanty, M. Misra, *Compos. Sci. Technol.* **2008**, *68*, 424–432.